JTTEE5 20:275–284
DOI: 10.1007/s11666-010-9595-8
1059-9630/$19.00 © ASM International

Consolidation of Al_2O_3/Al Nanocomposite Powder by Cold Spray

Dominique Poirier, Jean-Gabriel Legoux, Robin A.L. Drew, and Raynald Gauvin

(Submitted April 27, 2010; in revised form October 27, 2010)

While the improvement in mechanical properties of nanocomposites makes them attractive materials for structural applications, their processing still presents significant challenges. In this article, cold spray was used to consolidate milled Al and Al_2O_3/Al nanocomposite powders as well as the initial unmilled and unreinforced Al powder. The microstructure and nanohardness of the feedstock powders as well as those of the resulting coatings were compared. The results show that the large increase in hardness of the Al powder after mechanical milling is preserved after cold spraying. Good quality coating with low porosity is obtained from milled Al. However, the addition of Al_2O_3 to the Al powder during milling decreases the powder and coating nanohardness. This lower hardness is attributed to non-optimized milling parameters leading to cracked particles with insufficient Al_2O_3 embedding in Al. The coating produced from the milled Al_2O_3/Al mixture also showed lower particle cohesion and higher amount of porosity.

Keywords aluminum matrix composite, cold spray, nanostructured feedstock

1. Introduction

Owing to their lightweight and high specific strength, aluminum matrix composites are attractive structural materials for various domains such as automotive and aerospace applications. Recently, several authors have measured an increase in strength in aluminum or magnesium composites when the reinforcement size goes from microscale to nanoscale and it has also been reported that this strengthening is combined with an increase in ductility (Ref 1-6). On the other hand, the processing of composites with nanoreinforcement is not straight forward. In powder metallurgy, high energy mechanical milling was found to eliminate nanoparticle agglomeration and clustering issues for several composites (Ref 2, 7-9). In addition to homogeneous reinforcement dispersion, mechanical milling induces a significant grain size reduction, also beneficial to strength properties. However, the resulting milled powders were found to be difficult to consolidate. The compacts obtained by traditional consolidation methods such as hot pressing or extrusion display high porosity and poor particle bonding. Furthermore, the methods involving application of heat can lead to the loss of the nanograin structure as well as unwanted reactions (Ref 10, 11).

Cold spray consists of a coating production process with high-velocity particles at temperature significantly lower than the melting temperature of deposited materials. More information on this technique can be found elsewhere (Ref 12-15). Owing to the low temperatures involved in the process, cold spray can consolidate mechanically milled composite powders while preserving their nano grain size (Ref 16-19). For grains with size above the lower limit achievable by deformation, cold spray can even further refine the grains (Ref 19). Cold spray has also been used successfully to produce a few nanocomposites: dense coatings of TiB_2-Cu (Ref 20), TiN-Al (Ref 21), and Al_2O_3-Cu (Ref 22) have been obtained. In all the cases, the hardness of the nanocomposite coating was much higher than the hardness of the coating produced with the corresponding unreinforced and unmilled Cu or Al powder. However, milled Cu or Al powders were not included in the studies to distinguish the effect of milling from the effect of reinforcement addition on the powder sprayability and resulting coating properties.

The objective of this study is to compare the microstructure and properties of three cold-sprayed coatings. The first two were produced from mechanically milled powders: an Al_2O_3/Al nanocomposite mixture as well as an Al powder. The last coating was produced with the initial unreinforced and unmilled Al powder to serve as a reference. The effect of milling and reinforcement addition on the sprayability of the feedstock powder is discussed.

This article is an invited paper selected from presentations at the 2010 International Thermal Spray Conference and has been expanded from the original presentation. It is simultaneously published in *Thermal Spray: Global Solutions for Future Applications, Proceedings of the 2010 International Thermal Spray Conference*, Singapore, May 3-5, 2010, Basil R. Marple, Arvind Agarwal, Margaret M. Hyland, Yuk-Chiu Lau, Chang-Jiu Li, Rogerio S. Lima, and Ghislain Montavon, Ed., ASM International, Materials Park, OH, 2011.

Dominique Poirier and **Jean-Gabriel Legoux**, Industrial Materials Institute, National Research Council of Canada, Boucherville J4B 6Y4, Canada **Robin A.L. Drew**, Engineering and Computer Science, Concordia University, Montreal H3G 2W1, Canada; and **Raynald Gauvin**, Mining and Materials Engineering, McGill University, Montreal H3A 2B2, Canada. Contact e-mail: Dominique.Poirier@cnrc-nrc.gc.ca.

Evolution of powder nanohardness with milling, heat treatment and reinforcement addition is presented as well as the nanohardness of the resulting cold-sprayed coatings. The microstructure of the coatings was studied with an emphasis on the grain size evolution upon spraying.

2. Experimental

Spherical Al powder of −325 mesh, 99.5% purity, from Alfa Aesar (Ward Hill, USA) and Al_2O_3 of nominal size of 4 nm bought from Aldrich (St. Louis, USA) were used to produce the composite powders. Figure 1 shows the initial materials.

Two mechanically milled mixtures were produced, one from Al only and another one composed of 5 vol.% Al_2O_3/Al. Milling was performed in a Retsch (Haan, Germany) planetary mill PM200 with a ball-to-powder ratio of 7.5:1, a speed of 450 rpm and a milling time of 15 h under argon atmosphere. For ductile materials such as aluminum, a process control agent, stearic acid in this study, is added to the milling jar to prevent excessive welding. The appropriate powder size distribution for the cold spray technique was adjusted by varying the amount of stearic acid between 1.5 and 6 wt.%. The objective was to obtain a unimodal size distribution with an average as close as possible to 30 μm and a low amount of particles exceeding 60 μm (Ref 23). In the end, 4 wt.% stearic acid was selected, leading to an average size of around 35 μm and a particle morphology between equiaxed and flaky (Fig. 2). Figure 3 shows the size distribution of the milled powders.

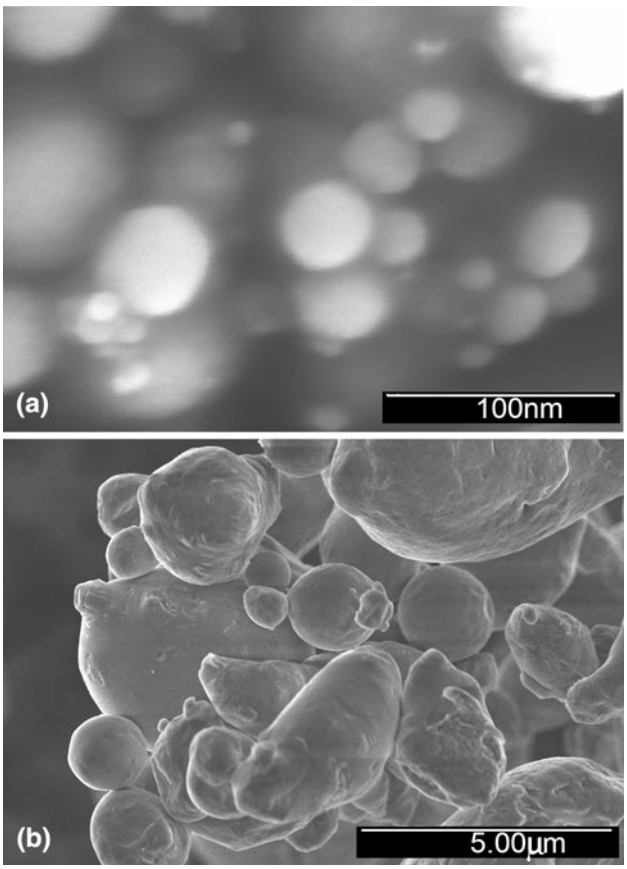

Fig. 1 SEM micrographs showing (a) Al_2O_3 powder and (b) initial Al powder

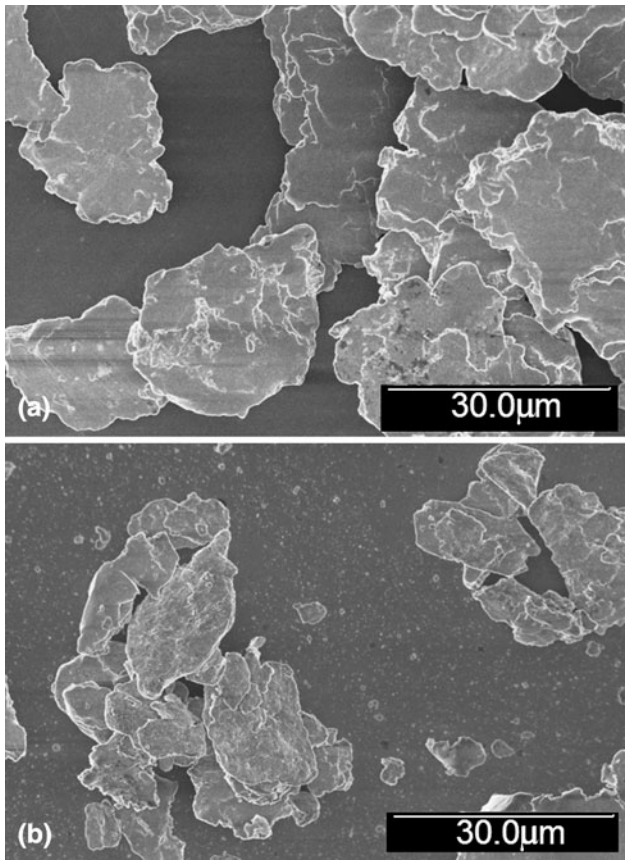

Fig. 2 SEM micrographs showing (a) milled Al and (b) milled Al_2O_3/Al mixtures for cold spraying

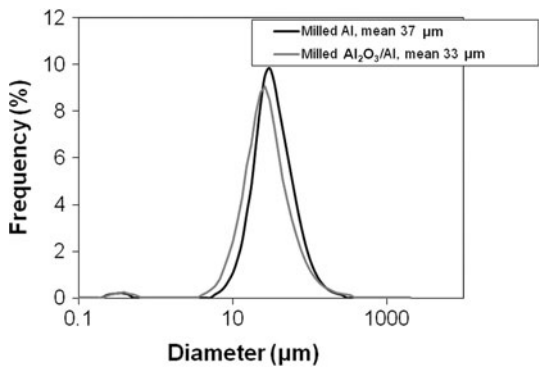

Fig. 3 Size distribution of milled Al and milled Al_2O_3/Al mixtures

Relatively high gas temperature, 500 °C, had to be used during cold spraying to favor powder deposition by increasing particle velocity. However, this high temperature can heat both the powder and the substrate (Ref 24), and it was unclear if the heat input during spraying could alter the microstructure of powders, and thus their properties. In order to avoid this effect and ease comparison between the properties of the powder feedstock and the coatings, the milled powders were heat treated (HT) at 450 °C for 15 min before cold spray.

The milled Al + HT and milled Al_2O_3/Al + HT powders as well as initial Al powder were cold sprayed on grit blasted (24 grit Al_2O_3) mild steel substrates 3 mm thick to produce three coatings. The final details for the cold spray process are as follows: Inovati cold spray system using Kinetic Metallization technology (a cold spray variant where a convergent nozzle is used to accelerate the process gas to Mach 1; Ref 12), inlet helium temperature and pressure of 500 °C (315 °C for initial Al) and 0.78 MPa, standoff distance of 2 cm, traverse speed of 10 mm/s (50 mm/s for initial Al), powder mass flow rate of about 5 g/min and 18 passes. The selection of those parameters is further discussed in section 3.

Morphology, size, and distribution of the Al_2O_3 and Al powders were studied using a field emission scanning electron microscope (FE-SEM) (Hitachi S-4700, Tokyo, Japan) and a particle size analyzer (Horiba LA-920, Tokyo, Japan). The cold spray coating microstructures in cross section were investigated with a SEM (Jeol JM-6100, Tokyo, Japan) after standard metallographic preparation. Phase change and precipitation were studied with a x-ray diffractometer (Bruker D8 Discover, Madison, USA). TEM (Philips CM200, Hillsboro, USA) was used to observe the second phase and to measure the grain size of the powders. For each sample, the Feret diameter of at least 30 grains was measured. Also, a TEM thin film of the cold-sprayed milled Al coating was prepared from grinding followed by electropolishing in a solution of 25% HNO_3 in methanol at −40 °C.

The nanohardness of powders and coating was evaluated using a nanoindentor (Nano G200 from MTS/Nano Instruments, Oak Ridge, USA) with a Berkovitch tip. 15-20 indents were conserved after filtration. Peak forces of 1 or 5 mN were selected with a hold time of 10 s. Nanohardness was calculated from the maximum load divided by the projected contact area. The reduced elastic modulus (E_r) was calculated from the stiffness based on the Oliver-Pharr data-analysis procedure (Ref 25). The reduced elastic modulus (E_r) was then converted to the Young's modulus from (Ref 25):

$$\frac{1}{E_r} = \frac{(1-\gamma^2)}{E} + \frac{(1-\gamma_i^2)}{E_i} \qquad \text{(Eq 1)}$$

where E and γ are, respectively, Young's modulus and Poisson ratio for the specimen, the latter being estimated as 0.33 (Ref 26). E_i and γ_i are the same parameters for the diamond indentor, taken to be 1141 GPa and 0.07, respectively from Ref 25.

3. Results and Discussion

3.1 Effects of Milling and Heat Treatment on Powders

Figure 4 shows the nanohardness obtained from the powders at various process stages as well as from the coatings. In order to minimize the effect of epoxy during indentation of the polished cross section of mounted powders, a very small load had to be used. This has somewhat increased scatter in the measured values. It has also introduced a bias toward higher hardness values. This trend, referred to as the indentation size effect, has been observed elsewhere (Ref 27-29). It is worth noting that the explanation for this phenomenon is still under debate. However, as a constant load was used for all the samples, the results can be compared with each other.

From Fig. 4, it is seen that milling increases the Al powder hardness by about 70%. Deformation occurring during milling leads to cold working and grain refinement (Ref 30). Also, various contaminants coming from the addition of the process control agent, wearing of the balls and vial, the initial oxide layers at the surface of the Al particles, or the extra oxidation occurring during the milling process, are embedded in the Al powder where they can form either a solid solution or dispersoids (Ref 31). All those phenomena contribute to the hardening observed after milling.

In the same graph, it can also be noticed that the milled Al powder nanohardness is increased after heat treatment. XRD patterns of the milled Al powders show an Al peak shift of 0.1° toward lower angles after heat treatment (Fig. 5). This shift is associated with a decrease in Al lattice parameters, probably from a lower amount of atoms in solid solution. Owing to the high energy involved in mechanical milling, this technique has been shown to produce various non-equilibrium alloy phases, such as supersaturated solid solution (Ref 31). Upon heating, the impurity atoms forming a supersaturated solid solution possibly precipitated out because of the increased diffusion rates to reduce the global energy of the system. It is

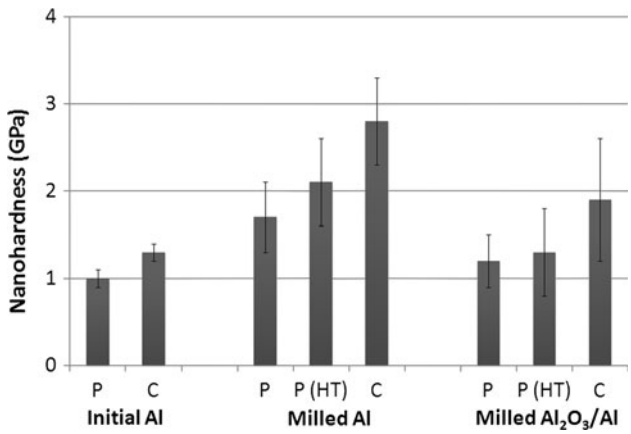

Fig. 4 Powder (P), heat treated powder (P(HT)) and coating (C) nanohardness at 1 mN load

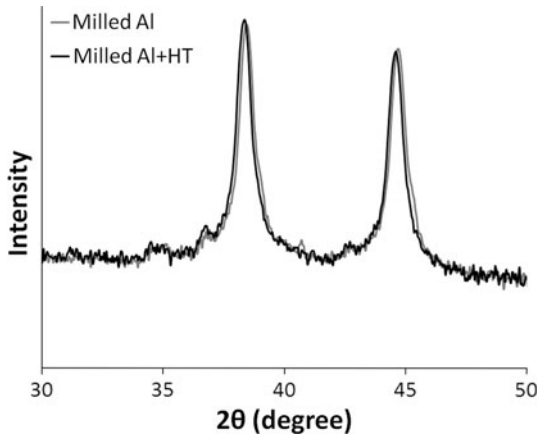

Fig. 5 XRD patterns of milled Al powders before and after heat treatment

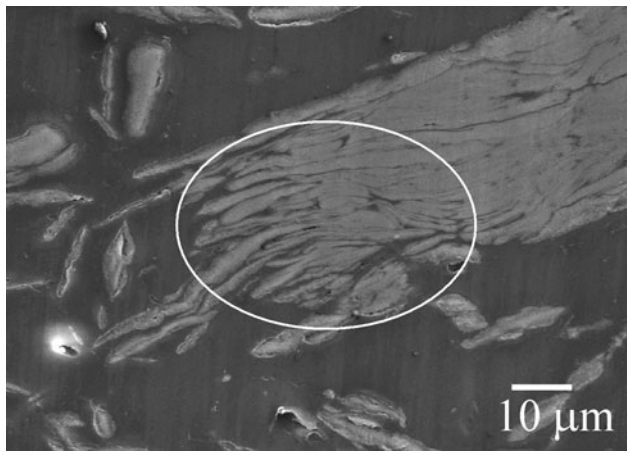

Fig. 6 Polished cross section of milled Al_2O_3/Al + HT powder

believed that this precipitation is the origin of the powder hardening after heat treatment. On the other hand, no sharpening of the peaks, indicating a possible annealing effect, was observed. It is supposed that the heat input during cold spray could have a similar effect on milled powders. This could lead to unusual trends such as a lower deposition efficiency with the use of a higher gas temperature. While a heat treatment was applied to all milled powders of this study to ease comparison between the properties of the powder feedstock and the coatings, an in-depth study of the effect of heat input during cold spraying could allow further understanding and optimization of the process.

If the hardness values of the milled Al + HT powder and the milled Al_2O_3/Al + HT powder are compared, then it can be seen that the former powder is harder. This was unexpected; Al_2O_3 was added with the purpose of reinforcing the Al. Previous study with the same initial constituents but different milling conditions indeed led to an increase in hardness with Al_2O_3 addition (Ref 11). It is believed that the modified milling parameters used in this study to accommodate cold spray requirements in terms of particle size and production yield did not allow optimized Al_2O_3 embedding and dispersion in Al powder. Figure 6 shows the polished cross section of milled Al_2O_3/Al + HT powder. Stacks of poorly welded particles are clearly seen, together with porosity and cracks. This lack of cohesion between lamellas could also lower hardness.

3.2 Spraying Parameters for Milled Powders

In order to cold spray a powder, the powder must first be fed to the nozzle. The flaky morphology of the milled particles reduced powder flow and made powder feeding impossible with the CGT Kinetic 3000 cold spray system. The effect of powder morphology on powder feeding has been studied by Gruner and Moens (Ref 32). This study showed that powders with an angular morphology have large surface-to-volume ratios which would make the powder feeding during thermal spray, including cold spray, difficult (bad powder flow and tendency to build up bridges, blockages, or pulsative powder flow). These problems were not observed with powders having a spherical morphology.

In order to favor powder flow, the Inovati cold spray system was selected mainly because its powder feeding system contains a brush that pushes powder inside the system. By using the highest mesh screen (20 mesh) and the hopper maximum speed (100%), a feeding rate of 5 g/min was achieved for milled Al + HT and 4.6 g/min for the milled Al_2O_3/Al + HT mixture. In comparison, the initial Al powder, with an equiaxed shape, only required 15% of the hopper speed for a feeding rate of 4.6 g/min. It is worth noting that powder deposition and coating quality might be restricted by the equipment maximum gas pressure of 0.9 MPa that limits particle velocity.

The second challenge encountered during cold spraying of milled powders is their higher hardness that reduces their ability to deform upon impact with the substrate (Ref 33). In this study, typical conditions led to no deposition. To favor deposition, the gas temperature was raised to the highest temperature allowable, 500 °C. By raising the gas temperature, the particle velocity is increased and the particle temperature also rises to allow more deformation upon impact. The traverse speed of the robot was also reduced to 10 mm/s to heat up the substrate (Ref 24). The efficiency of deposition stayed very low, with a value of 15% for milled Al + HT and 7% for the milled Al_2O_3/Al + HT. In comparison, the deposition efficiency of the initial Al was 43% with a lower gas temperature of 315 °C and a higher traverse speed of 50 mm/s.

It is worth noting that even if the milled Al_2O_3/Al + HT powder had a lower hardness than the milled Al + HT powder, it got a much lower deposition efficiency. Hardness measurements are affected by the cracks present in the Al_2O_3/Al + HT powder (Fig. 6), but the intrinsic material could actually be more resistant to deformation than the milled Al + HT powder. The Al_2O_3 particles could reduce the ductility of the powder locally, impeding proper deformation of the splat. Al_2O_3 at the surface of the Al powder could also impede physico-chemical reactions contributing to particle cohesion, in a fashion similar

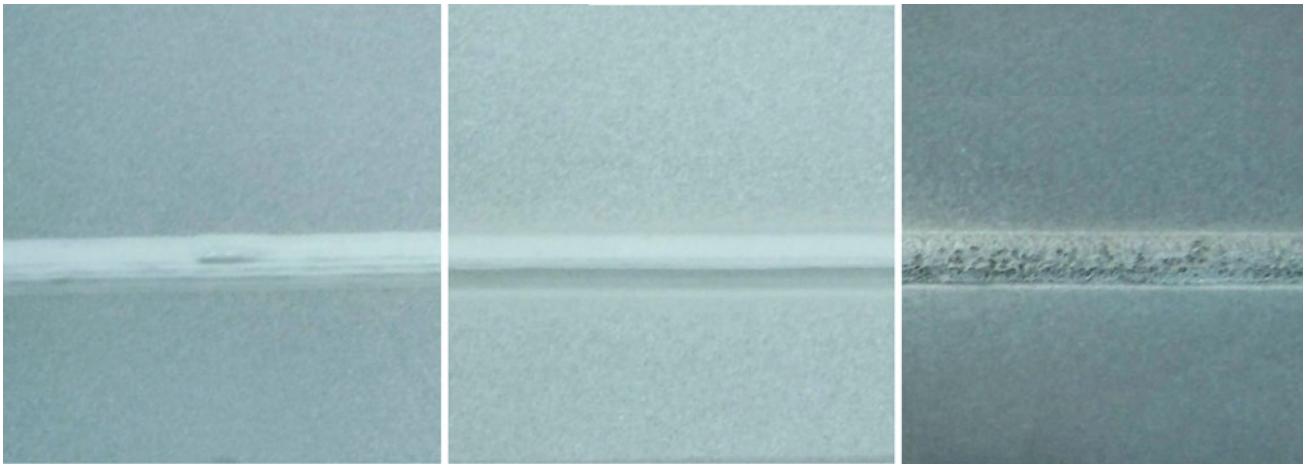

Fig. 7 Picture of the three coatings produced by cold spray. From left to right: initial Al, milled Al + HT, milled Al_2O_3/Al + HT

to what was observed elsewhere for surface impurities (Ref 34).

3.3 Coating Microstructures

The three coatings produced by cold spray are shown in Fig. 7. The coatings produced from the initial and the milled Al + HT powders are very similar. Those coatings are even and smooth. The coating made from the Al_2O_3/Al + HT mixture appears porous and brittle and was easily detached from the substrate. Furthermore, the mild steel substrate of this coating has darkened during the spraying process.

The microstructures of the three cold sprayed coatings are shown in Fig. 8. The coating produced from the initial Al powder is relatively dense: minimal porosity is visible. Its thickness is about 1.3 mm. As opposed to the milled Al + HT and milled Al_2O_3/Al + HT, the coating also remained strongly attached to the substrate through the cutting and mounting process involved in metallographic preparation, indicating a better adhesive strength. This also explains why the interface between the initial Al coating and the substrate is shown in Fig. 8(a) and (b), while the interfaces for the other two coatings could not be presented.

The milled Al + HT coating displays smaller but more numerous pores than the initial Al coating. While good quality coatings can be obtained with nanostructured feedstock, the porosity in the latter is always higher than in conventional coatings. The difference in porosity is explained by the higher hardness of the feedstock powder. Plastic deformation is limited and the generalized deformation required to fill all the cavities under the impacting particles is not experienced by the milled powder, resulting in a porous coating (Ref 18). This effect is even more obvious in this study, as the system used was limited to that of a low-pressure cold spray type, because of the poor feeding characteristics of the milled powders. It is worth noting that the use of high-pressure cold spray systems resulting in a higher powder velocity could compensate for the lower deformability of the milled powders. Figure 8(c) shows one of the few interlamellar cracks observed between traverse passes in the milled Al coating. Those cracks indicate a lack of bonding between adjacent deposited layers. By decreasing the robot traverse speed for milled powders, the amount of powder deposited for each traverse pass was increased. Because of the formation of the coating, the impingement angle for the particles of the subsequent pass was increased, leading to a lower normal velocity component. It is believed that the cracks result from the reduction in the extent of deformation because of the decreased normal velocity component (Ref 35). The thickness of this coating was about 2 mm, i.e., a higher value than the initial Al coating due to a lower traverse speed.

The milled Al_2O_3/Al + HT coating is half the thickness of the milled Al coating, i.e., about 1 mm, due to the poor deposition efficiency. The coating is very porous, cracked, and brittle, showing poor particle cohesion. A fractured cross section of the coating was also observed under FE-SEM. Figure 9 shows that the Al_2O_3 particles were indeed deposited in the coating. The embedding of the reinforcement in the matrix powder during mechanical milling should minimize loss of reinforcement during spraying. In Fig. 10, Al splats are clearly visible. The bonding between those splats seems to be weak. This lack of bonding could be due to the Al_2O_3 particles present at the surface of the Al splats that would impede physico-chemical interactions at the origin of cohesion. The numerous Al_2O_3 particles present at the surface of the splats rather than embedded within the Al could be due to insufficient milling.

Table 1 shows the evolution in grain size of the Al powder after milling, after heat treatment, and after cold spray. Milling did not refine the Al grains, of which the size remained at around 300 nm. Most probably, the milling parameters used in this study did not convey enough energy to cause the extensive deformation at the origin of grain refinement in the milling process. The heat treatment leads to some grain growth, resulting in a grain

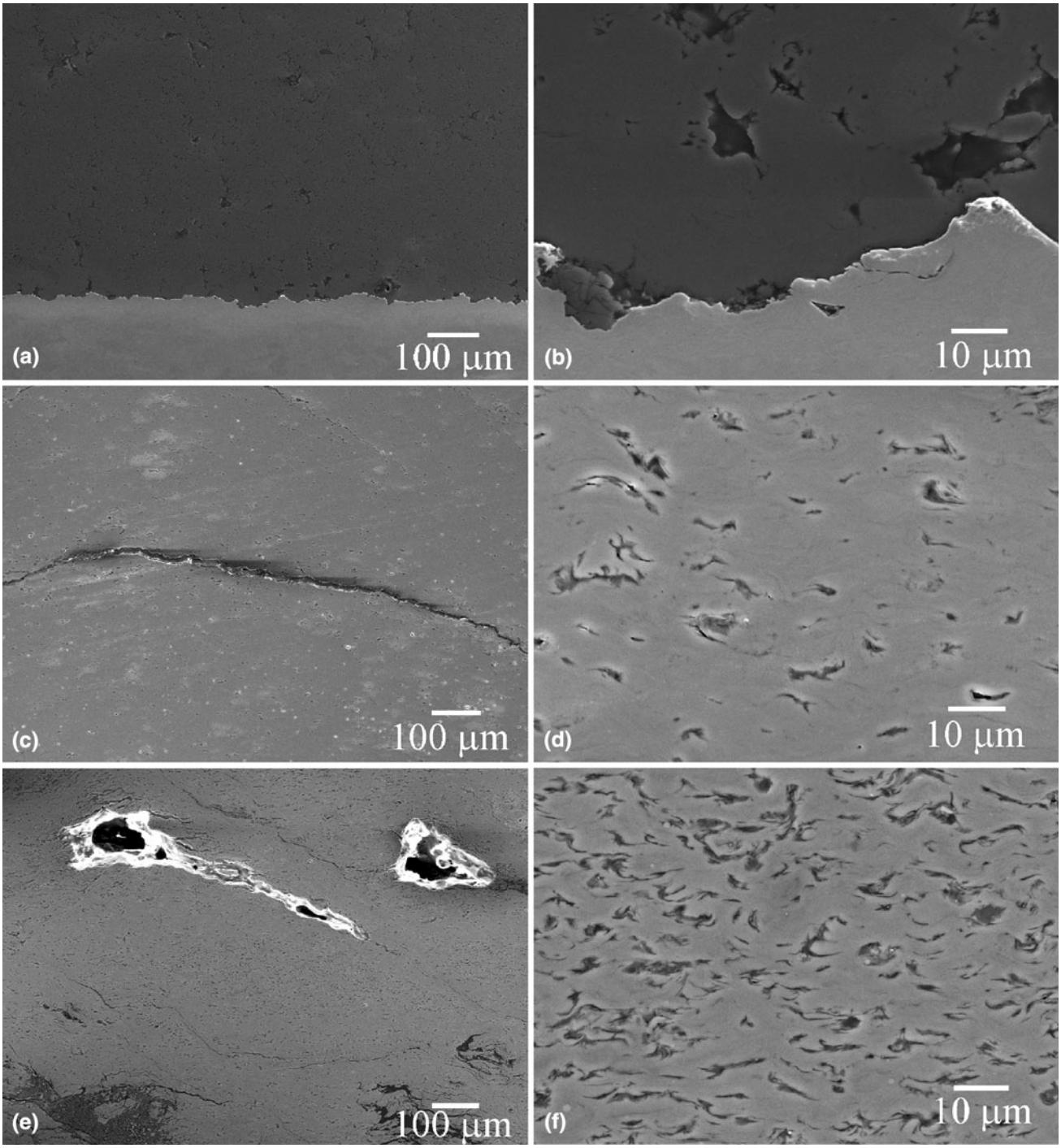

Fig. 8 Polished coating cross sections at two magnifications: (a, b) initial Al coating, (c, d) milled Al + HT coating, and (e, f) milled Al_2O_3/Al + HT coating

size of about 440 nm. A typical microstructure is shown in Fig. 11. Equiaxed grains are seen in the periphery of the particle of powder, where the sample is thinner and electron transparent.

After cold spray, the grains of the milled Al + HT coating are divided between fine and coarse grain regions. Figure 12 shows clearly visible coarse grains while a typical fine grain region is circled. The coarse grains have a size slightly higher than the milled Al powder after heat treatment. Owing to the high standard deviations, the variation might not be significant: more measurements would be needed to draw a clear conclusion. The TEM thin film was taken perpendicular to the substrate plane. The deposited particles are more likely to be deformed in

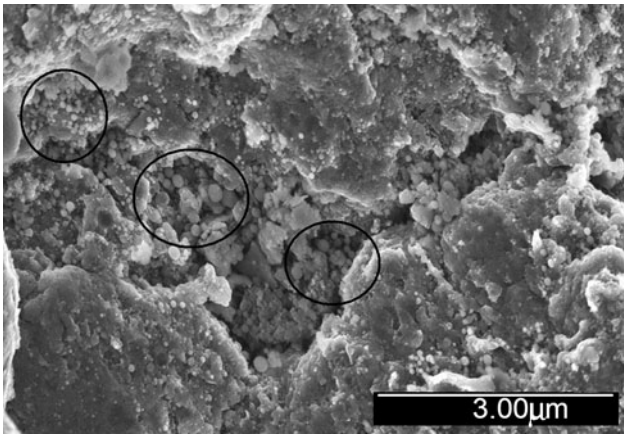

Fig. 9 SEM micrograph of the fractured cross section of the milled Al_2O_3/Al + HT coating showing the Al_2O_3 particles

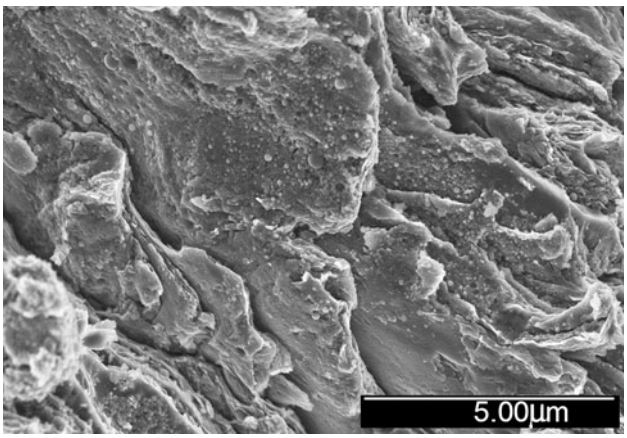

Fig. 10 SEM micrograph of the fractured cross section of the milled Al_2O_3/Al + HT coating showing the Al splats

Table 1 Grain sizes of milled Al coating and of its precursors

Material	Grain Feret's diameter, nm
Milled Al	300 ± 190
Milled Al after heat treatment	440 ± 240
Milled Al coating	Bimodal distribution • 90 ± 30 • 700 ± 270

the coating direction. Upon deformation, the grains of those regions might get slightly elongated in this direction, and thus appear slightly bigger. Some grain growth might also have occurred. The high gas temperature as well as the slow traverse speed of the robot has respectively favored the heating of the particles in flight and on the substrate.

In the same sample, fine grains are much smaller with a grain size of about 90 nm. While it was assumed for quite a long time that cold spray did not affect the microstructure, recent studies have shown that a grain refinement can occur (Ref 19, 36-38). This grain refinement is primarily

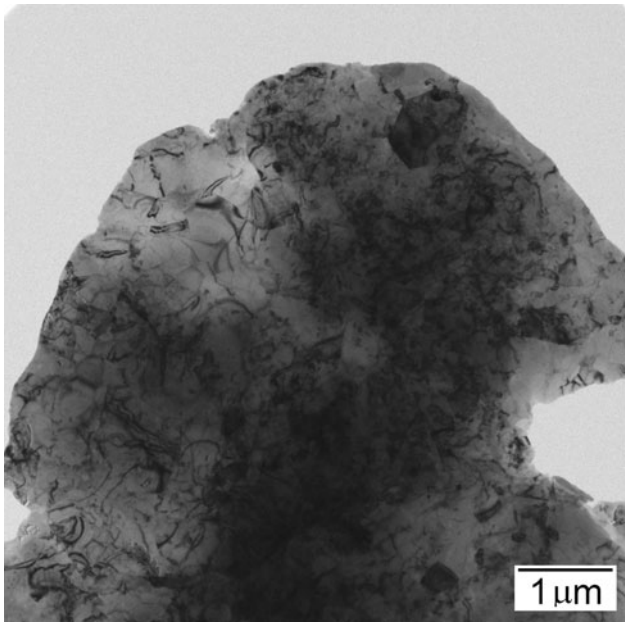

Fig. 11 TEM micrograph of the milled Al powder after heat treatment

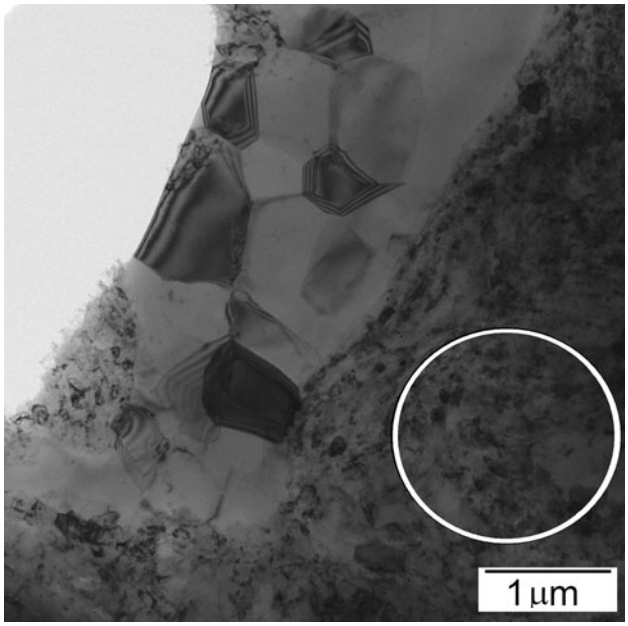

Fig. 12 TEM micrograph of the milled Al + HT coating showing a coarse grain region surrounded by fine grains

explained by the intensive deformation of the particles at the origin of their bonding in cold spray, but the exact mechanism is still unclear.

Figure 13 shows a region where elongated and curved grains were observed in the milled Al + HT coating. Those elongated grains are similar to those observed in adiabatic shear bands produced from high strain rate deformation (Ref 39). The existence of a non-uniform

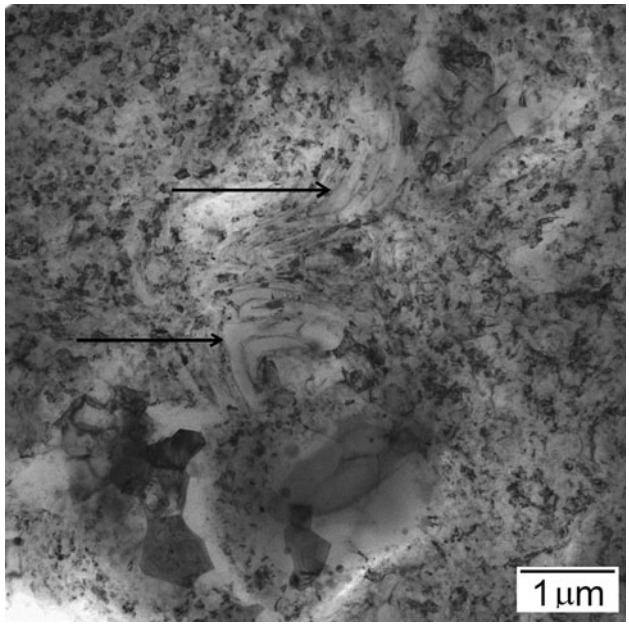

Fig. 13 TEM micrograph of the milled Al + HT coating where plastic deformation is visible through the elongated and deformed grains

coating microstructure composed of coarse, fine and elongated grains supports the adiabatic shear instability mechanism proposed for deformation occurring during cold spray. While the coarse grains would correspond to a particle region where very little deformation has occurred, as in the middle of the particle, the fine grains would correspond to areas of intensive plastic deformation where recrystallization has occurred, i.e., the regions of localized shearing at particle interfaces (Ref 36). The elongated and deformed grains would be intermediate regions were deformation has occurred, but not to an extent sufficient to trigger recrystallization.

The exact mechanism for grain recrystallization during cold spraying is believed to be similar to the other high-strain rate deformation process, i.e., some sort of dynamic recrystallization involving subgrain rotation. The strained and elongated grains would first have their dislocations reorganized in subgrains and cells in a relaxation process. With sufficient thermal energy, the dislocations would rearrange themselves in low angle grain boundaries that would eventually rotate to form high angle boundaries with more deformation (Ref 40).

3.4 Coating Hardness

Coating nanohardness can be compared with powder nanohardness in Fig. 4. For each powder type, a similar increase in hardness is observed after cold spraying. Part of this increase is probably due to the work hardening occurring during powder impact on the substrate. However, other factors might be involved, such as closing of cracks and porosity present in the milled powders upon impact deformation, grain refinement or removal of the epoxy compliance effect in the larger coating samples.

Table 2 Coating nanohardness and elastic modulus, 15 indents, 5 mN, DCM head

Coating	Nanohardness, GPa	Elastic Modulus, GPa
Initial Al	0.96 ± 0.09	83 ± 4
Milled Al + HT	2.1 ± 0.1	76 ± 3
Milled Al_2O_3 + HT	1.3 ± 0.3	82 ± 4

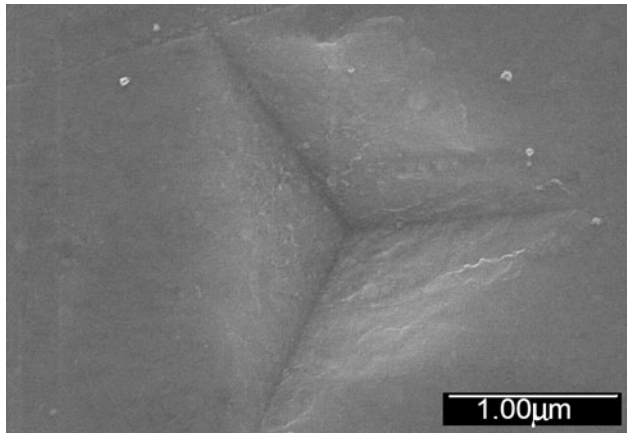

Fig. 14 SEM micrograph of a typical indent performed on the Al_2O_3/Al + HT coating

In order to improve accuracy, the coating nanohardness was also tested at a higher load and with the Dynamic Contact Module (DCM) head of the nanoindentor, with higher resolution. The results are displayed in Table 2. It can be seen that the elastic modulus is the same for the three coatings. This is as expected because the coating compositions are similar. It also means that the load used is small enough to avoid the effect of coating porosity. If this was not the case, then the elastic modulus of the Al_2O_3/Al + HT coating would be lower because of the higher porosity. Figure 14 shows a typical indent on the Al_2O_3/Al + HT coating. No crack is observed. In most cases, no pores were seen either. The elastic modulus values obtained are slightly higher than the Al Young's modulus measured through the tensile test (70 GPa; Ref 41) and similar to the values obtained by nanoindentation from another study (80 GPa; Ref 42).

Milling of the initial Al powder doubles the resulting Al coating nanohardness. The powder gain in hardness after milling is, therefore, preserved after cold spraying. The higher gas temperature used for the spraying of milled powders compared with the gas temperature used for the initial Al powder could also play a role. As a higher gas temperature results in higher particle velocity, the particles could deform more upon impact, increasing the extent of cold working.

The Al_2O_3/Al + HT coating displays a higher nanohardness than the initial Al coating, but a lower nanohardness than the milled Al coating. The nanohardness trend of the powders is then reflected in the coating and it can be expected that Al_2O_3/Al + HT coating hardness could be much improved with feedstock of higher quality.

4. Conclusions

In this study, the microstructure and properties of three Al-based cold sprayed coatings were compared. The first two coatings were produced from mechanically milled powders: an Al_2O_3/Al nanocomposite mixture as well as an Al powder. The last coating was produced with the initial unreinforced and unmilled Al powder to serve as a reference. It was found that milling increases Al powder hardness by about 70%. The subsequent heat treatment further increases the hardness of the milled powders by precipitation hardening. The resulting powders exhibit low deformability and necessitate high process gas temperature and low traverse speed to obtain cold spray deposition of relatively dense coatings. TEM observations of milled Al coatings have shown that recrystallization had occurred in the regions of high plastic deformation, forming nanograins. Those regions would correspond to the regions of localized shearing at the particle interfaces in accordance with the adiabatic shear instability mechanism. Also, it was found that the gain in hardness of the Al powder due to milling is preserved in the coating after cold spraying.

However, the addition of Al_2O_3 to the milled powder further decreases deposition efficiency and leads to porous and brittle coatings, with lack of bonding between particles. The Al_2O_3/Al + HT mixture displays improved hardness compared to the initial Al powder. Yet, its hardness is lower than the milled Al powder hardness because of the presence of cracks in the particles as well as poor Al_2O_3 embedding and dispersion. In that case, the lower deposition efficiency of the milled Al_2O_3/Al + HT mixture could be explained by a local reduction of the powder deformability at the Al_2O_3 particle vicinity. Furthermore, the presence of Al_2O_3 at the surface of Al particles could impede the physico-chemical reactions needed for proper bonding of an incoming particle.

References

1. Y.-C. Kang and S.L.-I. Chan, Tensile Properties of Nanometric Al_2O_3 Particulate-Reinforced Aluminum Matrix Composites, *Mater. Chem. Phys.*, 2004, **85**(2-3), p 438-443
2. Z.R. Hesabi, A. Simchi, and S.M.S. Reihani, Structural Evolution During Mechanical Milling of Nanometric and Micrometric Al_2O_3 Reinforced Al Matrix Composites, *Mater. Sci. Eng. A*, 2006, **428**(1-2), p 159-168
3. Z.Y. Ma, Y.L. Li, Y. Liang, F. Zheng, J. Bi, and S.C. Tjong, Nanometric Si_3N_4 Particulate-Reinforced Aluminum Composite, *Mater. Sci. Eng. A*, 1996, **219**(1-2), p 229-231
4. S.F. Hassan and M. Gupta, Effect of Particulate Size of Al_2O_3 Reinforcement on Microstructure and Mechanical Behavior of Solidification Processed Elemental Mg, *J. Alloys Compd.*, 2006, **419**(1-2), p 84-90
5. S.F. Hassan, M.J. Tan, and M. Gupta, High-Temperature Tensile Properties of Mg/Al_2O_3 Nanocomposite, *Mater. Sci. Eng. A*, 2008, **486**(1-2), p 56-62
6. M. Sherif El-Eskandarany, Mechanical Solid State Mixing for Synthesizing of SiCp/Al Nanocomposites, *J. Alloys Compd.*, 1998, **279**(2), p 263-271
7. J. Naser, W. Riehemann, and H. Ferkel, Dispersion Hardening of Metals by Nanoscaled Ceramic Powders, *Mater. Sci. Eng. A*, 1997, **234-236**, p 467-469
8. H. Ferkel and B.L. Mordike, Magnesium Strengthened by SiC Nanoparticles, *Mater. Sci. Eng. A*, 2001, **298**(1-2), p 193-199
9. F. Tang, M. Hagiwara, and J.M. Schoenung, Microstructure and Tensile Properties of Bulk Nanostructured Al-5083/SiCp Composites Prepared by Cryomilling, *Mater. Sci. Eng. A*, 2005, **407** (1-2), p 306-314
10. C.C. Koch, Synthesis of Nanostructured Materials by Mechanical Milling: Problems and Opportunities, *Nanostruct. Mater.*, 1997, **9**(1-8), p 13-22
11. D. Poirier, R. Gauvin, and R. Drew, Al-Al_2O_3 Nanocomposites Produced by Mechanical Milling, *Advances in Powder Metallurgy and Particulate Materials*, June 28-July 1, 2009 (Las Vegas), MPIF, 2009
12. E. Irissou, J.G. Legoux, A.N. Ryabinin, B. Jodoin, and C. Moreau, Review on Cold Spray Process and Technology. Part I. Intellectual Property, *J. Therm. Spray Technol.*, 2008, **17**(4), p 495-516
13. V.K. Champagne, *The Cold Spray Materials Deposition Process: Fundamentals and Applications*, Woodhead Publishing Limited, 2007, 376 p
14. A. Papyrin, V. Kosarev, K.V. Klinkov, A. Alkhimov, and V.M. Fomin, *Cold Spray Technology*, A. Papyrin, Ed., Elsevier, 2006, 328 p
15. R.G. Maev and V. Leshchinsky, *Introduction to Low Pressure Gas Dynamic Spray: Physics & Technology*, Wiley-VCH Verlag GmbH, 2008, 234 p
16. L. Ajdelsztajn, B. Jodoin, G.E. Kim, and J.M. Schoenung, Cold Spray Deposition of Nanocrystalline Aluminum Alloys, *Metall. Mater. Trans. A*, 2005, **36**, p 657-666
17. B. Jodoin, L. Ajdelsztajn, E. Sansoucy, A. Zuniga, P. Richer, and E.J. Lavernia, Effect of Particle size, Morphology, and Hardness on Cold Gas Dynamic Sprayed Aluminum Alloy Coatings, *Surf. Coat. Technol.*, 2006, **201**, p 3422-3429
18. L. Ajdelsztajn, A. Zuniga, B. Jodoin, and E.J. Lavernia, Cold-Spray Processing of a Nanocrystalline Al-Cu=Mg-Fe-Ni Alloy with Sc, *J. Therm. Spray Technol.*, 2006, **15**(2), p 184-190
19. A.C. Hall, L.N. Brewer, and T.J. Roemer, Preparation of Aluminum Coatings Containing Homogeneous Nanocrystalline Microstructures Using the Cold Spray Process, *J. Therm. Spray Technol.*, 2008, **17**(3), p 352-359
20. J.S. Kim, Y.S. Kwon, O.I. Lomovsky, D.V. Dudina, V.F. Kosarev, S.V. Klinkov, D.H. Kwon, and I. Smurov, Cold Spraying of In Situ Produced TiB2-Cu Nanocomposite Powders, *Compos. Sci. Technol.*, 2007, **67**, p 2292-2296
21. W.-Y. Li, G. Zhang, O. Elkedim, H. Liao, and C. Coddet, Effect of Ball Milling of Feedstock Powder on Microstructure and Properties of TiN Particle-Reinforced Al Alloy-Based Composites Fabricated by Cold Spray, *J. Therm. Spray Technol.*, 2008, **17**(3), p 316-322
22. P. Sudharshan Phani, V. Vishnukanthan, and G. Sunderarajan, Effect of Heat Treatment on Properties of Cold Sprayed Nanocrystalline Copper Alumina Coatings, *Acta Mater.*, 2007, **55**, p 4741-4751
23. L. Ajdelsztajn, B. Jodoin, G.E. Kim, and J.M. Schoenung, Cold spray Deposition of Nanocrystalline Aluminum Alloys, *Metall. Mater. Trans. A*, 2005, **36**(3), p 657-666
24. E. Irissou, J.-G. Legoux, C. Moreau, and A.N. Ryabinin, How Cold is Cold Spray? An Experimental Study of the Heat Transfer to the Substrate in Cold Gas Dynamic Spraying, *Thermal Spray Crossing Borders*, E. Lugscheider, Ed., June 2-4, 2008 (Maastricht), ASM International, 2008, 1604 p
25. W.C. Oliver and G.M. Pharr, An Improved Technique for Determining Hardness and Elastic Modulus Using Load and Displacement Sensing Indentation Experiments, *J. Mater. Res.*, 1992, **7**(6), p 1564-1583
26. T.W. Clyne and P.J. Withers, *An Introduction to Metal Matrix Composites*, Cambridge University Press, New York, 1993, 492 p
27. J. Gong, H. Miao, Z. Peng, and L. Qi, Effect of Peak Load on the Determination of Hardness and Young's Modulus of Hot-Pressed Si_3N_4 by Nanoindentation, *Mater. Sci. Eng. A*, 2003, **354**(1-2), p 140-145
28. X. Shi, H. Yang, G. Shao, X. Duan, and Z. Xiong, Nanoindentation Study of Ultrafine WC-10Co Cemented Carbide, *Mater. Character.*, 2008, **59**(4), p 374-379

29. B. Yang and H. Vehoff, Dependence of Nanohardness upon Indentation Size and Grain Size—A Local Examination of the Interaction Between Dislocations and Grain Boundaries, *Acta Mater.*, 2007, **55**(3), p 849-856
30. A. Khan, D. Farrokh, and L. Takacs, Effect of Grain Refinement on Mechanical Properties of Ball-Milled Bulk Aluminum, *Mater. Sci. Eng. A*, 2008, **489**, p 77-84
31. C. Suryanarayana, Mechanical Alloying and Milling, *Prog. Mater. Sci.*, 2001, **46**(1-2), p 1-184
32. P.G.H. Gruner and J. Moens, Optimized Powder Feeding, a Key Parameter for Thermal Spraying, *Thermal Spray Connects: Explore Its Surfacing Potential!*, E. Lugscheider, Ed., May 2-4, 2005 (Basel), ASM International, 2005, p 1558-1560
33. A.Z.L. Ajdelsztajn, B. Jodoin, and E.J. Lavernia, Cold Spray Processing of a Nanocrystalline Al-Cu-Mg-Fe-Ni Alloy with Sc, *J. Therm. Spray Technol.*, 2006, **15**, p 184-190
34. D.K. Christoulis, F. Borit, V. Guipont, and M. Jeandin, Evidence of the 2-Stage Build-Up Process in Cold Spray from the Study of Influence of Powder Characterisation, *Thermal Spray Crossing Borders*, E. Lugscheider, Ed., June 2-4, 2008 (Maastricht), ASM International, 2008, 1604 p
35. W. Wong, S. Yue, E. Irissou, and J. Legoux, Influence of Helium and Nitrogen Gases on the Properties of Cold Gas Dynamic Sprayed Pure Titanium Coatings, *J. Therm. Spray Technol.* doi:10.1007/s11666-010-9568-y
36. P. Richer, A. Zúñiga, M. Yandouzi, and B. Jodoin, CoNiCrAlY Microstructural Changes Induced During Cold Gas Dynamic Spraying, *Surf. Coat. Technol.*, 2008, **203**(3-4), p 364-371
37. C.-J. Li, W.-Y. Li, and Y.-Y. Wang, Formation of Metastable Phases in Cold-Sprayed Soft Metallic Deposit, *Surf. Coat. Technol.*, 2005, **198**(1-3), p 469-473
38. C. Borchers, F. Gartner, T. Stoltenhoff, H. Assadi, and H. Kreye, Microstructural and Macroscopic Properties of Cold Sprayed Copper Coatings, *J. Appl. Phys.*, 2003, **93**(12), p 10064-10070
39. J.F.C. Lins, H.R.Z. Sandim, H.J. Kestenbach, D. Raabe, and K.S. Vecchio, A Microstructural Investigation of Adiabatic Shear Bands in an Interstitial Free Steel, *Mater. Sci. Eng. A*, 2007, **457**(1-2), p 205-218
40. K. Kim, M. Watanabe, J. Kawakita, and S. Kuroda, Grain Refinement in a Single Titanium Powder Particle Impacted at High Velocity, *Scripta Mater.*, 2008, **59**(7), p 768-771
41. W.D. Callister, *Materials Science and Engineering; An Introduction*, 5th ed., John Wiley and Sons, New York, 2000, 871 p
42. R. Rodriguez and I. Gutierrez, Correlation Between Nanoindentation and Tensile Properties; Influence of the Indentation Size Effect, *Mater. Sci. Eng. A*, 2003, **361**, p 377-384